Available online at www.sciencedirect.com
ScienceDirect
Journal of Catalysis 243 (2006) 340–349
JOURNAL OF CATALYSIS
www.elsevier.com/locate/jcat

# The synergy between Fe and Ru in $N_2O$ decomposition over FeRu-FER catalysts: A mechanistic explanation

Gerhard D. Pirngruber [a,*,1], Lukas Frunz [a], Johannis A.Z. Pieterse [b]

[a] *Institute for Chemical and Bioengineering, ETH Zurich, CH-8093 Zurich, Switzerland*
[b] *ECN Hydrogen & Clean Fossil Fuels, PO Box 1, Westerduinweg 3, 1755 ZG, Petten, The Netherlands*

Received 10 May 2006; revised 8 August 2006; accepted 12 August 2006

**Abstract**

Fe-FER is an active catalyst for the abatement of $N_2O$ in the tail gas of nitric acid plants. The activity of Fe-FER can be increased if Ru is added as a second active component. This is a surprising finding, because noble metals are usually strongly inhibited by NO, which is always present in tail gas. Yet the bimetallic FeRu-FER catalyst is more active than the sum of the components, Fe-FER and Ru-FER. A synergy between Fe and Ru can explain this phenomenon. This work discusses the role of Fe and Ru in the reaction mechanism as well as the interplay of these two components. In situ IR measurements show that the preferential adsorption of NO and its reaction products on Fe in the bimetallic catalyst reduces the inhibiting effect of NO on the Ru component; this effect largely contributes to the synergy between Fe and Ru. Moreover, in situ X-ray absorption data are presented, which allow for tracing the average oxidation state of the two active components Fe and Ru under reaction conditions.


*Keywords:* In situ spectroscopy; NO adsorption; XANES; IR; Ferrierite

## 1. Introduction

Direct catalytic decomposition of $N_2O$ in the tail gases of nitric acid plants is a safe, cost-efficient method for $N_2O$ abatement. Consequently, much effort is invested in developing improved catalysts that convert $N_2O$ at moderate temperatures (below 773 K). Iron zeolites, especially Fe-ZSM-5, have been studied extensively for use as catalysts in $N_2O$ decomposition [1–5]. $NO_x$, which is usually present in off-gases, promotes $N_2O$ decomposition over iron zeolites [6–9]. Fe-FER [4,10] and Fe-BEA [5] perform particularly well. However, a temperature of 773 K is still necessary to achieve 75% $N_2O$ conversion with Fe-FER in the presence of $H_2O$ and $NO_x$ [10]. Noble metal catalysts have a higher intrinsic activity for $N_2O$ decomposition compared with iron [11]. Unfortunately, $N_2O$ decomposition over noble metal catalysts is inhibited by NO, $O_2$, and $H_2O$ [12,13], precluding their use in the tail gas of nitric acid factories. Recently it was shown that using a bimetallic FER catalyst containing iron and ruthenium significantly enhances $N_2O$ decomposition if some NO is present [14,15]. This effect also manifests in the presence of $O_2$ and $H_2O$. The bimetallic catalyst is more active than the sum of the single components, Fe and Ru; there is a synergy between Fe and Ru [16]. Possible explanations for this synergy have been offered [15], but the effect remains incompletely understood. The goal of the present contribution is to unravel the mechanism by which Fe and Ru cooperate, with the aid of in situ spectroscopy (IR and XANES).

## 2. Experimental

### 2.1. Catalyst preparation

$NH_4$-FER was obtained from Na/K-FER (Tosoh HSZ-720KOA, Si/Al = 9.2) by threefold ion exchange with a $NH_4NO_3$ solution for 1 h at room temperature. The sample was filtered and washed with a large amount of demineralized

* Corresponding author.
*E-mail address:* gerhard.pirngruber@ifp.fr (G.D. Pirngruber).
[1] Present address: Catalysis and Separation Division, Institut Français du Pétrole, 69390 Vernaison, France.

0021-9517/$ – see front matter 
doi:10.1016/j.jcat.2006.08.006

Table 1
Elemental composition of the samples and intensity of Brønsted OH band

| Sample | Fe (wt%) | Ru (wt%) | Fe/Al | Ru/Al | (Na + K)[a]/ Al | Exchange Brønsted OH (%) |
|---|---|---|---|---|---|---|
| Fe-FER | 2.2 | n.d.[b] | 0.31 | – | – | 17 |
| FeRu-FER | 2.2 | 0.4 | 0.31 | 0.03 | 0.22 | 32 |
| Ru-FER | n.d. | 0.4 | – | 0.03 | 0.29 | 28 |
| Fe-FER-2 | 0.6 | n.d. | 0.09 | – | – | 20 |
| FeRu-FER-2 | 0.6 | 0.45 | 0.09 | 0.04 | 0.73 | 68 |
| Ru-FER-2 | n.d. | 0.45 | – | 0.04 | n.d. | 68 |

[a] Mainly K, only traces of Na.
[b] n.d. = not determined.

water to remove nitrate. Fe-FER (2.2 wt% Fe) was prepared by impregnating $NH_4$-FER with iron nitrate.

Ru-FER was obtained by exchanging $Ru(NH_4)_3Cl_6$ with 25 g Na/K-FER at 353 K for 16 h (nominal Ru loading, 0.5%; initial pH, 8; final pH, 6.5), followed by two exchanges with 0.05 M $NH_4NO_3$ for 1 h. The purpose of the treatment with $NH_4NO_3$ was to maximize the exchange capacity for the subsequent impregnation with iron nitrate (vide infra). The final Ru loading was determined by ICP to be 0.40 wt%.

FeRu-FER was obtained by incipient-wetness impregnation of Ru-FER with a solution of iron nitrate, to obtain 2.2 wt% Fe. The samples were calcined under flowing air at 793 K for 3 h (at a ramp of 3 K/min).

A second batch of Ru-FER (coded as Ru-FER-2) was prepared at a larger scale, in which 100 g of Na/K-FER was exchanged with $Ru(NH_4)_3Cl_6$ for 16 h at 353 K. The sample was washed and filtered, followed by a single exchange with 0.05 M $NH_4NO_3$ for 1 h. The final loading was determined by ICP to be 0.45 wt% Ru. FeRu-FER-2 was obtained by incipient-wetness impregnation of Ru-FER-2 (0.45 wt% Ru) with a more diluted solution of iron nitrate to obtain 0.6 wt% Fe. Similarly, Fe-FER-2 was obtained by impregnation of $NH_4$-FER with a diluted solution to obtain 0.6 wt% Fe (Table 1).

The samples were characterized by UV–vis, TPR, IR, and XANES/EXAFS spectroscopy. UV–vis spectra were recorded on a Cary 400 UV–vis spectrometer with a Praying Mantis sample stage from Harrick. $H_2$-TPR spectra were recorded with an Altamira AMI-1 apparatus equipped with a thermal conductivity detector and a Balzers MS-detector, applying 30 ml/min flow of 10% $H_2$ in argon at a heating rate of 20 K/min. IR and XAS are explained in more detail below. The elemental composition of the samples was determined by ICP or AAS (for Na and K).

### 2.2. Activity measurements

The catalytic tests were conducted in a computer-controlled six-flow setup. First, 50 mg of catalyst (sieve fraction, 0.25–0.5 mm) was placed on a quartz grid, then the quartz reactors (4 mm i.d.) were placed in an oven. The total gas flow was 100 ml/min, corresponding to a GHSV of ∼60,000 $h^{-1}$. Quantitative analysis of the gas-phase components was performed using a micro-gas chromatograph and a $NO_x$ analyzer. Data were collected at ascending temperatures from 533 to 773 K (ramp 5 K/min). Preconditioning was set for 20 min at each temperature. Pseudo-first-order rate constants were calculated using the formula

$$k = -\frac{F}{m_{\text{cat}} \cdot p} \cdot \ln(1 - X),$$

where $F$ is total flow, $m_{\text{cat}}$ mass of the catalyst, $p$ is total pressure, and $X$ is the conversion. The equilibrium between NO and $NO_2$ was calculated using HSC software.

### 2.3. In situ IR spectroscopy

A 6-mg catalyst sample was pressed into a self-supporting pellet, placed in a gold sample holder, and inserted in the in situ IR cell [17]. The sample was heated in a flow of 5% $O_2$ in He to 673 K and kept there for 30 min, to remove all impurities. Subsequently, the cell was purged for 30 min in He flow at 673 K to facilitate autoreduction of the catalyst. The cell was cooled to 573 K. A spectrum of the catalyst was recorded and used as a reference for the subsequent measurements. The reaction was started by switching from He to a mixture of ∼3000 ppm $N_2O$, ∼800 ppm NO, and 0–2% $O_2$. The concentration of NO and $N_2O$ was twice as great as in the catalytic tests described above. The range of the mass flow controllers imposed this choice. The gas flow was kept at 20 $ml_{NTP}$/min, corresponding to a GHSV of ∼100,000 $h^{-1}$. After ∼30 min (once steady state was reached), the gas inlet was switched back to He, the catalyst was regenerated at 673 K for 30 min, and the procedure was repeated at the next reaction temperatures (i.e., 623 and 673 K). The IR spectra were recorded on a Biorad FTS 3000 MX spectrometer equipped with a broadband MCT detector. The spectral resolution was 4 $cm^{-1}$. A total of 16–128 scans were co-added. 16 scans correspond to a time resolution of ∼10 s. The reactor effluent was analyzed by mass spectrometry [17]. To remove impurities of $NO_2$ in the feed, the NO/He mixture was passed through a cold trap at 173 K.

### 2.4. In situ XANES spectroscopy

The in situ XANES measurements were performed at beamline BM26 (DUBBLE) at ESRF, Grenoble. An EXAFS cell dedicated for in situ measurements in the fluorescence mode was used [18]. A 10-mg catalyst sample was gently pressed into the sample compartment through which the gas flow passes. An Al foil (99.999% purity, 15 μm thickness) was used to seal the sample and also served as the window for the EXAFS radiation. A double-crystal Si(111) monochromator selected the energy of the X-rays, and a nine-channel monolithic Ge detector was used to collect the fluorescence radiation. Measurements were performed at both the Fe $K$-edge and the Ru $K$-edge. The scan time was ∼8 min.

In the standard procedure, the sample was heated in 3% $O_2$ in He to 673 K and kept at that temperature for 30 min. After the cell was flushed in He for 30 min, three different reactions were performed: (i) 3000 ppm $N_2O$ + 800 ppm NO, (ii) 3000 ppm $N_2O$ + 800 ppm NO + 2% $O_2$, and (iii) 5000 ppm $N_2O$ and the balance He. Each reaction was performed in situ for 30 min, followed by purging in He for 30 min. The

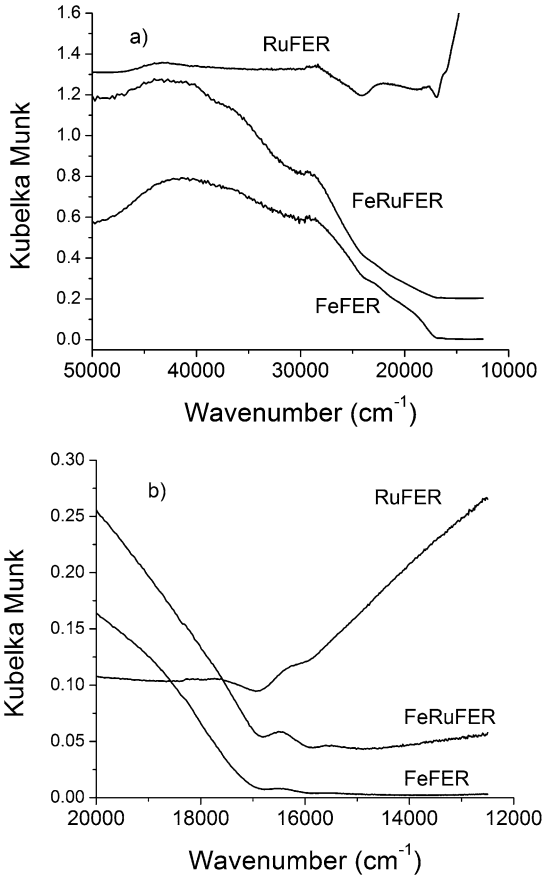


Fig. 1. (a) UV–vis spectra of Fe-FER, FeRu-FER and Ru-FER. (b) Zoom on the low wavenumbers. Spectra are offset for better visibility.

total gas flow was 17.5 $ml_{NTP}$/min, corresponding to GHSV ~53,000 $h^{-1}$, and the reaction temperature was 673 K. The reactor effluent was analyzed by mass spectrometry. After the reaction sequence was completed, Fe-FER was reduced in $H_2$ at 673 K, to generate a reference spectrum of a fully reduced $Fe^{2+}$ sample.

## 3. Results

### 3.1. Characterization

The Fe/Al ratio of Fe-FER is 0.31, corresponding to an exchange degree of 62% (Table 1). Yet the Brønsted OH band at 3590 $cm^{-1}$ loses only 17% of its intensity compared with the parent H-FER sample. This effect is due to the impregnation method used, which results in physical deposition of iron on the surface rather than to a true ion exchange. The UV–vis spectra of Fe-FER shows an intense band at 29,000 $cm^{-1}$ in addition to the typical O → Fe LMCT transitions at 42,000 and 36,500 $cm^{-1}$ (Fig. 1). The band at 29,000 $cm^{-1}$ is characteristic of oligonuclear iron species [19,20]. Additional shoulders at 23,000 and 20,000 $cm^{-1}$ demonstrate that the sample also contains larger $Fe_2O_3$ particles, which are probably deposited on the outer surface of the zeolite during impregnation. The presence of $Fe_2O_3$ was confirmed by $H_2$-TPR showing that a considerable fraction of the iron sites reduced at very high temperatures (Fig. 2) similar to the reduction for $Fe_2O_3$ [21]. The $H_2$/Fe consumption up to 1050 K is 0.90. Assuming that this figure results from a mixture of large $Fe_2O_3$ clusters that reduce to $Fe^0$ and of other isolated or oligonuclear iron species that reduce only to $Fe^{2+}$, we can deduce that the fraction of $Fe_2O_3$ should be 40%.

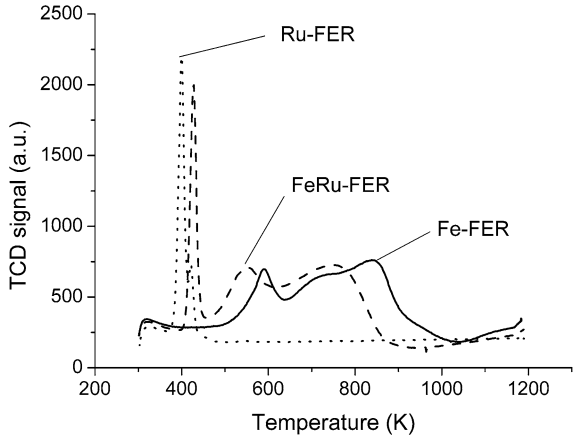


Fig. 2. $H_2$-TPR of Fe-FER, FeRu-FER and Ru-FER.

Ru-FER has a rather weak Brønsted OH-band despite the low Ru/Al ratio, because the sample still contains $Na^+$ and $K^+$ counter ions (Table 1). The UV–vis spectrum of Ru-FER (Fig. 1) is similar to that of $RuO_2$; its features can be explained by the band structure of $RuO_2$ [22]. The strong absorption below 17,000 $cm^{-1}$ is due to absorptions within the conduction band, composed of Ru 4d orbitals. The transitions at higher energies (i.e., 28,500 and 43,500 $cm^{-1}$) can be assigned to transitions from the valence band (i.e., from O 2p orbitals) to the conduction band. Compared with crystalline $RuO_2$, these are strongly red-shifted, due to the reduction of the band gap as a result of the small cluster size [23]. The EXAFS/XANES spectrum of Ru-FER is very similar to that of a $RuO_2$ reference sample. In the Fourier-transformed EXAFS spectrum, the similarity extends up to 4 Å, corresponding to two complete coordination shells. From this, we can deduce that the average size of the $RuO_2$ clusters should be at least 1–2 nm.

The UV–vis absorption of Ru-FER is much weaker than that of Fe-FER; thus, it is not surprising that the UV–vis spectrum of FeRu-FER more closely resembles Fe-FER than Ru-FER. However, closer inspection of the low-energy region of the spectrum shows that FeRu-FER also exhibits free electron absorption within the conduction band, which is typical for $RuO_2$ clusters (Fig. 1b). The TPR spectrum of FeRu-FER is similar to that of Fe-FER, but with an additional peak at low temperature due to the reduction of ruthenium (Fig. 2). The subsequent reduction of iron shifts to lower temperatures because Ru aids the reduction.

Fe-FER-2 was prepared by incipient wetness impregnation of a more dilute iron nitrate solution than Fe-FER. In contrast to Fe-FER, Fe-FER-2 is colorless. Its UV–vis spectrum (not shown) exhibits only the two LMCT transitions at 42,000 and 36,500 $cm^{-1}$. Oligonuclear iron species are absent in this sample. Although the iron loading is three times lower than that in

Table 2
Pseudo first order rate constants of $N_2O$ decomposition in a feed of 1500 ppm $N_2O$, 400 ppm NO, 0 or 2% $O_2$[a]

| $T$ (K) | $k$ (mmol/(s g bar)) | | | | | |
|---|---|---|---|---|---|---|
| | With $O_2$ | | | Without $O_2$ | | |
| | Ru-FER | Fe-FER | FeRu-FER | Ru-FER | Fe-ER | FeRu-FER |
| 652 | 0.00 | 0.30 | 0.45 | 0.09 | 0.35 | 0.86 |
| 672 | 0.03 | 0.49 | 0.81 | 0.24 | 0.57 | 1.40 |
| 692 | 0.12 | 0.76 | 1.44 | 0.49 | 0.89 | 2.25 |
| 722 | 0.35 | 1.48 | 2.93 | 1.19 | 1.65 | 3.96 |

[a] GHSV = 60,000 $h^{-1}$, $p = 1$ bar.

Fe-FER-2, the fraction of exchanged Brønsted sites is similar (Table 1). This confirms that a large part of the additional iron in Fe-FER is not exchanged with Brønsted sites, but is only deposited on the catalyst.

### 3.2. $N_2O$ decomposition activity

The main results of the catalytic tests with the first batch of samples were presented earlier [15] and are only summarized here. The $N_2O$ decomposition activity in a feed of 1500 ppm $N_2O$ + 400 ppm NO (+2% $O_2$) increases in the order Ru-FER < Fe-FER < FeRu-FER. The pseudo-first-order rate constants of FeRu-FER are higher than the sum of the two other catalysts (Table 2). Adding $O_2$ to the feed decreases the activity of all three catalysts; the inhibiting effect of $O_2$ decreases in the order Ru-FER > FeRu-FER ≫ Fe-FER. The $NO_2$ concentration profiles show some interesting differences between the catalysts (Fig. 3). $NO_2$ can be formed by one of two reactions:

$$NO + (1/2)O_2 \rightarrow NO_2 \quad (1)$$

or

$$NO + N_2O \rightarrow NO_2 + N_2. \quad (2)$$

Reaction (1) is equilibrium-limited, but reaction (2) is not. Its $\Delta G_r^0$ at 673 K is −135 kJ/mol. When $O_2$ is present in the feed, Ru-FER and FeRu-FER establish the equilibrium between NO and $NO_2$ above 570 and 590 K, respectively (Fig. 3). On Fe-FER, the $NO_2$ concentration exceeds the NO/$NO_2$ equilibrium, because the source of $NO_2$ is mainly reaction (2). The $NO_2$ formation reaches its maximum at 685 K. At higher temperatures, $NO_2$ is rapidly consumed by reaction with $N_2O$, and its concentration decreases (vide infra).

In the absence of $O_2$, Ru-FER is not active for $NO_2$ formation. Fe-FER forms little $NO_2$ at low temperatures, demonstrating that $NO_2$ formation at these temperatures is due mainly to reaction (1). Reaction pathway (2) is hardly affected by the presence or absence of $O_2$. The $NO_2$ profile of Fe-FER at high temperatures is very similar to the one in the presence of $O_2$. FeRu-FER behaves like Fe-FER at low temperatures. The $NO_2$ concentration reaches a maximum at 595 K and then approaches the equilibrium $NO_2 \rightarrow NO + (1/2)O_2$; that is, the NO/$NO_2$ ratio shifts towards NO with increasing temperature. Fig. 3 does not show the NO concentration, but because the sum of NO and $NO_2$ is constant at 400 ppm, the profile of NO can be deduced.

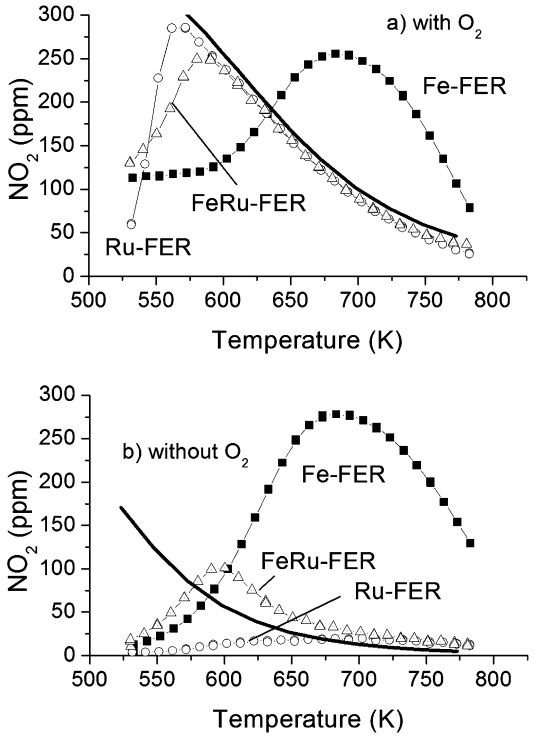


Fig. 3. $NO_2$ concentration profile during NO decomposition with 1500 ppm $N_2O$, 400 ppm NO and (a) 2 or (b) 0% $O_2$ over Fe-FER (■), FeRu-FER (△), Ru-FER (○). Solid lines represent equilibria (a) NO + (1/2) $O_2 \rightarrow NO_2$ (feed 400 ppm NO + 2% $O_2$) and (b) $NO_2 \rightarrow$ NO + (1/2)$O_2$ (feed 400 ppm $NO_2$).

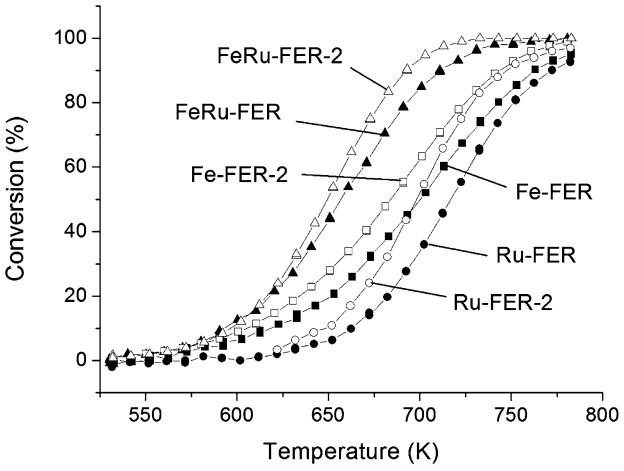


Fig. 4. $N_2O$ conversion in a feed of 1500 ppm $N_2O$, 400 ppm NO, balance $N_2$. GHSV = 60000 $h^{-1}$, $p = 1$ bar.

The catalysts of the second batch are more active than those of the original preparation (Fig. 4). The higher activity of Fe-FER-2 compared with Fe-FER confirms that a large fraction of iron in Fe-FER does not participate in the reaction. The higher activity of Ru-FER-2 compared with Ru-FER can be attributed to slight differences in the preparation procedures. As for the first batch, the first-order rate constants of FeRu-FER-2 are larger than the sum of Fe-FER-2 and Ru-FER-2 (see Table 3).

Table 3
Pseudo first order rate constants of $N_2O$ decomposition in a feed of 1500 ppm $N_2O$ and 400 ppm NO[a]

| $T$ (K) | $k$ (mmol/(s g bar)), without $O_2$ | | |
|---|---|---|---|
| | Ru-FER-2 | Fe-FER-2 | FeRu-FER-2 |
| 652 | 0.17 | 0.49 | 1.14 |
| 672 | 0.41 | 0.79 | 2.06 |
| 692 | 0.84 | 1.22 | 3.49 |
| 722 | 2.12 | 2.25 | 6.85 |

[a] GHSV = 60,000 $h^{-1}$, $p = 1$ bar.

### 3.3. In situ IR spectroscopy in absence of $O_2$

Fig. 5 shows the IR spectra of Fe-FER during reaction with NO + $N_2O$ at 573 K. An intense nitrosyl band at 1866 $cm^{-1}$ appears almost immediately after switching to the reaction mixture. After 1 min, its intensity gradually decreases to a steady-state value. A band at 1625 $cm^{-1}$ slowly increases in intensity and reaches steady state after ∼15 min. It is accompanied by a broad shoulder at 1550 $cm^{-1}$. Both bands can be assigned to nitro/nitrate species [24,25]. The doublet at 2238 and 2205 $cm^{-1}$ is due to gas-phase $N_2O$. The intensity of the $N_2O$ band seems to increase over time. The increase is due to a broad band of $NO^+$ hidden below the $N_2O$ doublet. The $NO^+$ band becomes visible when switching from the reaction mixture back to He. In the region of the OH stretching vibrations, a band at 3646 $cm^{-1}$ and a shoulder at 3605 $cm^{-1}$ appear, which can be assigned to Fe–OH stretching vibrations [26]. The negative band at 3575 $cm^{-1}$ is due to the replacement of Brønsted protons by $NO^+$ [27]. The nitrosyl band rapidly disappears on switching back to He. The $NO^+$ band and the corresponding negative Brønsted OH band disappear within a few minutes; however, the Fe–OH and the nitrate/nitro bands are stable and decrease very slowly over time. The spectra at 623 K are very similar, but the nitrosyl band is much weaker. At 673 K, the intensity of the nitrosyl band is zero, and only nitrates are observed.

Fig. 6 shows the corresponding spectra with Ru-FER. Some differences can be immediately observed. No OH-groups are created, and the negative band of the Brønsted OH groups is much less intense. Likewise, the $NO^+$ band is missing. The nitrosyl band is at a different wavelength (i.e., 1876 $cm^{-1}$), and the nitro/nitrate band is shifted to 1634 $cm^{-1}$. In contrast to Fe-FER, the nitrosyl band is rather stable and decreases only after several minutes of He purging. The nitro/nitrate band is also very stable during the He purge. The spectra at higher temperatures are almost identical to those at 573 K. The intensity of the nitrosyl and nitro band hardly decreases, indicating the high stability, particularly of the nitrosyl group, on the $RuO_2$ surface. The high stability of the surface nitrosyl is probably at the heart of the inhibiting effect of NO on decomposition activity of Ru-FER.

The objective of the study was to compare the behavior of the bimetallic catalyst with the single components Fe-FER and Ru-FER. Fig. 7 shows the IR spectra of all three samples measured in steady state at 573 and 623 K. The spectra of FeRu-FER resemble those of Fe-FER with respect to band intensity, band position, and shape. The similarity of Fe-FER and FeRu-FER is also observed in the time-on-stream behavior (see Fig. 8). Both Fe-FER and FeRu-FER show a rapid initial increase of the nitrosyl band, followed by a decrease of the intensity between 1 and 5 min, which is ascribed to the oxidation of NO species to $NO_x$. This effect is not observed for Ru-FER. During He purging, the nitrosyl species desorb very

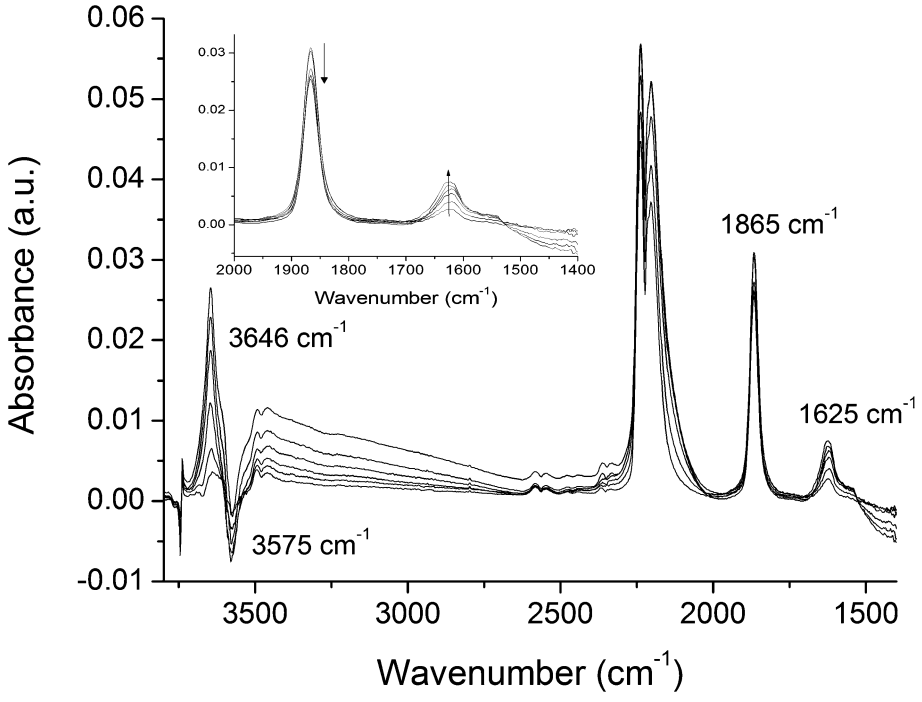


Fig. 5. IR spectra measured during reaction of Fe-FER with NO + $N_2O$ at 573 K, after 0.5, 1, 2, 4, 8 and 18 min on stream.

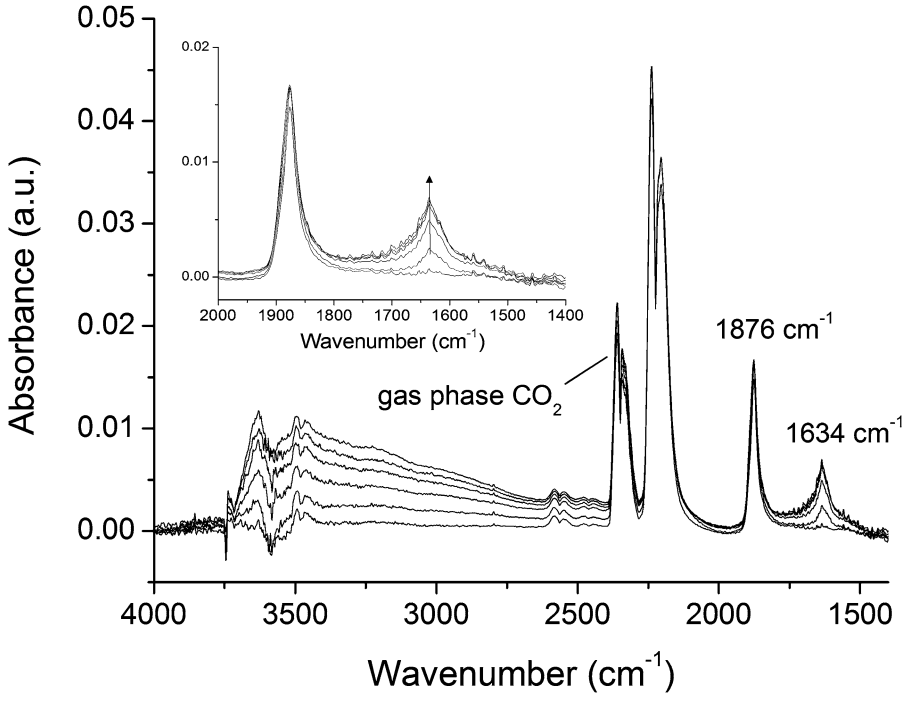


Fig. 6. IR spectra measured during reaction of Ru-FER with NO + $N_2O$ at 573 K, after 0.5, 1, 2, 4, 8 and 18 min on stream. The bands of gas phase $CO_2$ are an artifact that originates from the air in the spectrometer compartment.

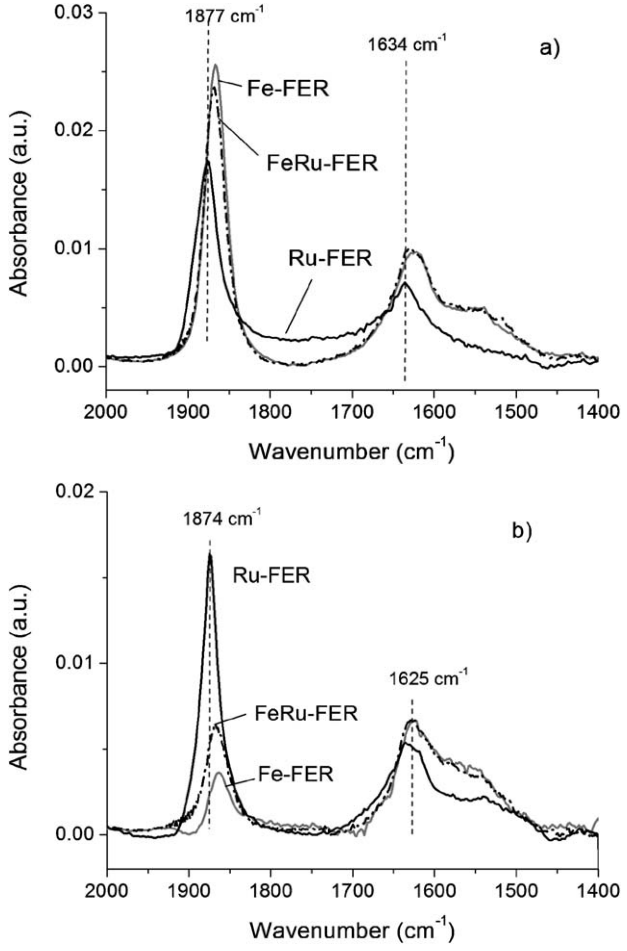


Fig. 7. IR spectra of Fe-FER (—), Ru-FER (—) and FeRu-FER (-·-·-) at (a) 573 K and (b) 623 K after 30 min reaction with NO + $N_2O$.

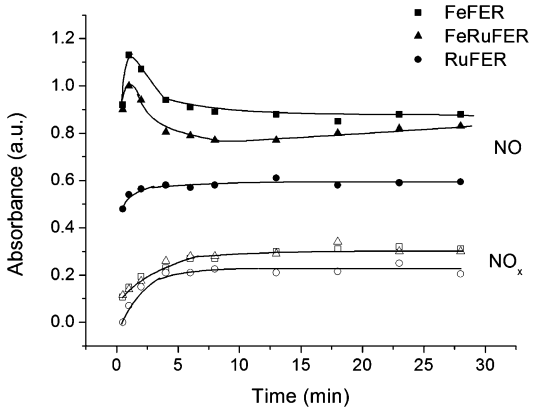


Fig. 8. Intensity of the NO (1866 or 1877 $cm^{-1}$, full symbols) and of the nitro/nitrate bands (1625 or 1635 $cm^{-1}$, open symbols) as a function of time on stream during the reaction of the catalysts with NO + $N_2O$ at 573 K.

rapidly from Fe-FER and FeRu-FER, whereas the intensity of the NO band decreases only gradually in Ru-FER (see Fig. 9), due to the higher stability of the nitrosyl species adsorbed on Ru. In conclusion, we can state that the bimetallic catalyst behaves like Fe-FER in the in situ IR experiments.

### 3.4. *In situ IR spectroscopy in the presence of $O_2$*

Fig. 10 compares the IR spectra of Fe-FER in the presence and absence of $O_2$ in the feed. In the presence of $O_2$, the intensity of the surface nitrosyl band on Fe-FER decreases, and the nitro groups increase in intensity. Among the nitro bands, a band at 1575 $cm^{-1}$ becomes particularly more intense. This band was observed earlier during the reaction of NO with $O_2$ on iron zeolites [28,29]. Moreover, the intensity of the Fe–

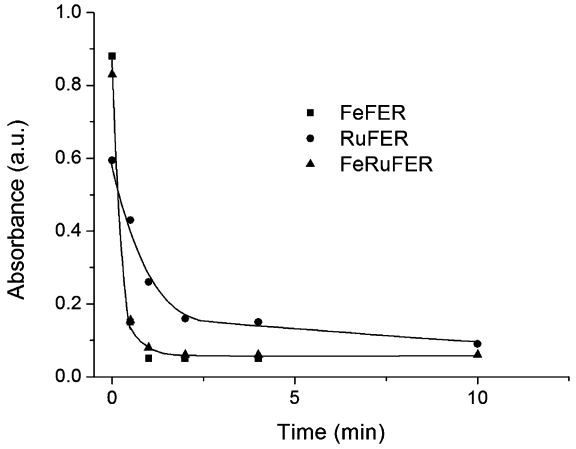


Fig. 9. Intensity of the NO band (1866 or 1877 $cm^{-1}$) as function of time during the He purge, after reaction of the catalysts with NO + $N_2O$ at 573 K.

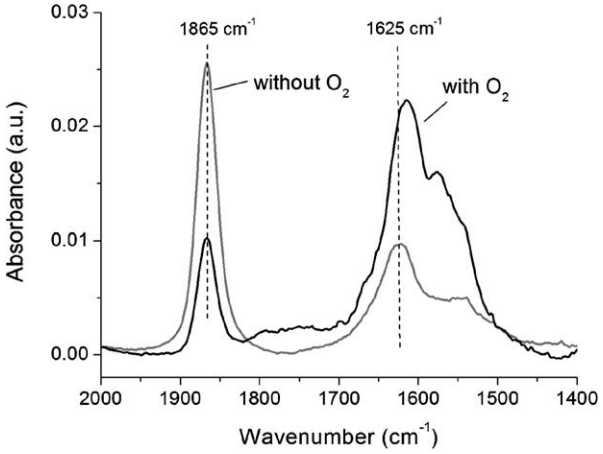


Fig. 10. IR spectra of Fe-FER after 30 min reaction with NO + $N_2O$ at 573 K, in the presence and absence of $O_2$.

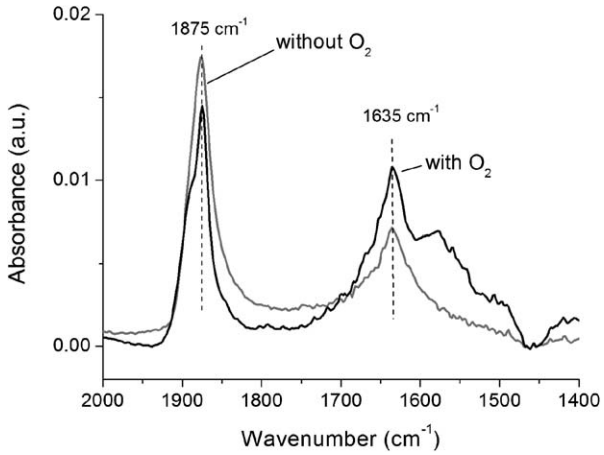


Fig. 11. IR spectra of Ru-FER after 30 min reaction with NO + $N_2O$ at 573 K in the presence and absence of $O_2$.

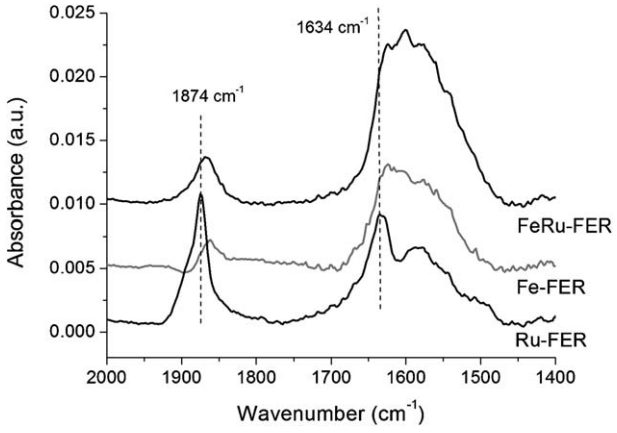


Fig. 12. IR spectra of Fe-FER, Ru-FER and FeRu-FER at 623 K after 30 min reaction with NO + $N_2O$ + $O_2$.

OH groups increases slightly compared with the reaction without $O_2$. Because the Fe–OH groups arise from the oxidation of $Fe^{2+}$ to $Fe^{3+}$, it is not surprising that their intensity increases in the presence of $O_2$.

The situation is similar for FeRu-FER. Compared with the reaction without $O_2$, the nitrosyl band decreases and the nitro bands (particularly a band at 1575 $cm^{-1}$) increase in intensity. For Ru-FER, the nitro bands also increase (Fig. 11), and a second NO band at 1890 $cm^{-1}$ becomes visible. The higher frequency of the NO stretching vibration indicates less back-donation from Ru to the NO $2\pi^*$ antibonding orbital. In the presence of $O_2$, the $RuO_2$ surface is more oxidized (i.e., the electron density at the Fermi level is reduced) and thus less willing to donate electrons to NO [30]. Surprisingly, the total intensity of the nitrosyl band decreases by only 15% compared with that in the reaction without $O_2$. We attribute this to the fact that NO- and $NO_2$-derived species are in chemical equilibrium on the $RuO_2$ surface. The ratio between surface nitrosyl and surface nitro species shifts in favor of NO with increasing temperature, as does the equilibrium between NO and $NO_2$ in the gas phase. The presence of $O_2$ increases the total concentration of the surface $NO/NO_2$ species and shifts the equilibrium toward the $NO_2$-derived species, but the equilibrium remains in favor of NO.

For FeRu-FER, shape and position of the NO and $NO_x$ bands in the presence of $O_2$ are similar to those of Fe-FER. At 573 K, the nitrosyl band has similar intensity on all three catalysts. The absorbance of the nitro/nitrate bands decreases in the order FeRu-FER > Fe-FER > Ru-FER (not shown). The spectra of the three samples at 623 K are shown in Fig. 12. As in the absence of $O_2$, the Ru-FER catalyst maintains a rather intense nitrosyl band at 623 K, whereas the nitrosyl band of Fe-FER and FeRu-FER is weak. The intensity of the nitro/nitrato bands is highest on FeRu-FER, probably due to the higher fraction of $Fe^{3+}$ sites in FeRu-FER (see Section 3.5). We can postulate that the NO adsorption on FeRu-FER is similar to that on Fe-FER, also when $O_2$ is present in the feed.

The spectra of the three samples of the second batch are shown in Fig. 13. The region of nitrate/nitro bands is better resolved, and a number of additional bands appear. We do not discuss or assign these bands in detail here; for our purposes, the important information is that the spectra of FeRu-FER-2 do not resemble those of Fe-FER-2. The intensity and position of the nitrosyl band in the bimetallic sample are closer to those of Ru-FER-2. The band is very stable and desorbs only

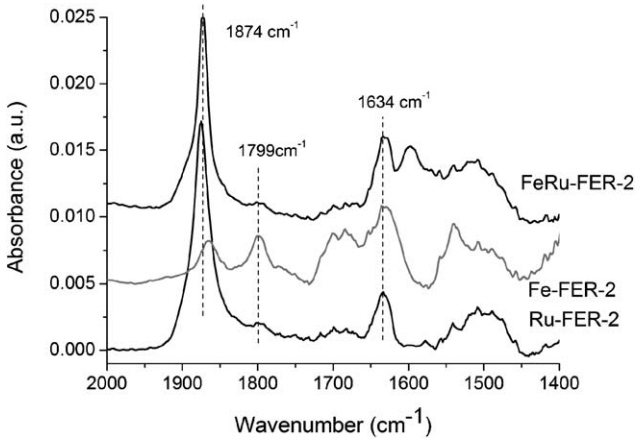


Fig. 13. IR spectra of Fe-FER-2, Ru-FER-2 and FeRu-FER-2 at 623 K after 30 min reaction with NO + $N_2O$ + $O_2$.

very slowly in He. We can postulate that in FeRu-FER-2, NO adsorbs on the ruthenium component rather than on the iron component.

### 3.5. In situ XANES spectroscopy

The in situ XANES measurements were carried out to follow the changes in the oxidation state of the catalyst during pretreatment, reaction, and regeneration. Fe-FER contains a large amount of large $Fe_2O_3$ clusters, which dominate the X-ray absorption. These clusters do not reduce easily and do not participate in the reaction. Hence, only very small shifts of the Fe *K*-edge are seen in the in situ experiments. A quantitative comparison of the redox behavior of Fe-FER and FeRu-FER is, therefore, not possible. To circumvent the dominating contribution of the large $Fe_2O_3$ clusters on the X-ray absorption spectra, a second batch of Fe-FER (i.e., Fe-FER-2) was prepared that does not contain oligonuclear iron clusters or $Fe_2O_3$ particles. Fe-FER-2 exhibits a high redox activity during the in situ XANES measurements. Fig. 14 shows the in situ XANES spectra of Fe-FER-2 in the three reaction mixtures $N_2O$ + NO, $N_2O$ + NO + $O_2$, and $N_2O$, as well as after reduction in $H_2$. The spectrum in $N_2O$ corresponds to the fully oxidized state ($Fe^{3+}$); the spectrum in $H_2$, to the fully reduced state ($Fe^{2+}$). The fully reduced form has a characteristic peak in the edge at 7118.5 eV. The spectra measured during reaction with $N_2O$ + NO (+ $O_2$) correspond to mixed oxidation states. The fraction of oxidized iron sites was determined by linear combination of the reference spectra in $N_2O$ and $H_2$. During reaction with NO + $N_2O$, approximately 30% of the iron sites are reduced to $Fe^{2+}$ (Table 4). The fraction of reduced sites during reaction hardly depends on the presence or absence of $O_2$. Note that $O_2$ does not inhibit $N_2O$ decomposition over Fe-FER. Autoreduction of $Fe^{3+}$ to $Fe^{2+}$ occurs when purging with He before switching to another reaction mixture. The fraction of reduced sites in He is about 40%.

The same analysis was performed for FeRu-FER-2 (Table 4). During reaction with NO + $N_2O$, FeRu-FER-2 has a similar fraction of $Fe^{2+}$ sites as seen in Fe-FER-2. When $O_2$ is added to the reaction mixture, the concentration of $Fe^{2+}$ decreases. Catalytic results indeed show a small inhibiting effect of $O_2$ on the bimetallic catalyst (Table 2), which may be ascribed to the lower concentration of $Fe^{2+}$ sites (vide infra). The comparison of Fe-FER-2 and FeRu-FER-2 reveals that the bimetallic catalyst reduces less readily than the iron sample.

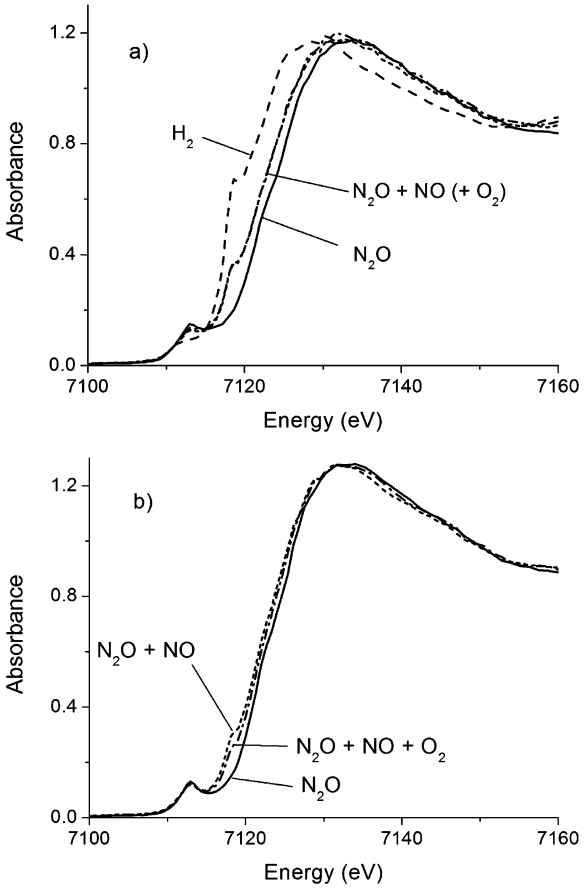


Fig. 14. In situ XANES spectra of (a) Fe-FER-2 and (b) FeRu-FER-2 during reaction with $N_2O$ + NO (- - -), $N_2O$ + NO + $O_2$ (·····), $N_2O$ only (—) and after reduction in $H_2$ (– – –), at 673 K.

Table 4
Fraction of $Fe^{2+}$ sites during pretreatment in $O_2$, autoreduction in He and reaction with NO + $N_2O$ (+ $O_2$) at 673 K

| | Fe-FER-2 | FeRu-FER-2 |
|---|---|---|
| $O_2$ | ~50 | 19 |
| He[a] | 55 | 31 |
| NO + $N_2O$ | 33 | 27 |
| He[b] | 42 | 30 |
| NO + $N_2O$ + $O_2$ | 31 | 18 |
| He[c] | 40 | 29 |

[a] He purge after treatment with $O_2$.
[b] He purge after reaction with NO + $N_2O$.
[c] He purge after reaction with NO + $N_2O$ + $O_2$.

## 4. Discussion

### 4.1. Catalytic synergy

To set the basis for discussing the spectroscopic data, we briefly recall what is already known about the catalytic properties of iron and ruthenium ferrierite. The mechanism of $N_2O$

decomposition on iron zeolites in the presence of NO can be described by the following set of equations:

$$N_2O + NO \rightarrow NO_2 + N_2, \quad (2)$$

$$N_2O + NO_2 \rightarrow NO + N_2 + O_2, \quad (3)$$

$$\text{Sum:} \quad 2N_2O \rightarrow 2N_2 + O_2.$$

NO functions as intermediate oxygen storage [6–8,31]. It takes up oxygen from $N_2O$ and is converted to $NO_2$. $NO_2$ releases the oxygen atom again by reaction with a second molecule of $N_2O$, and $O_2$ is formed. This mechanism greatly enhances the rate of $O_2$ formation, which otherwise is a very slow step in $N_2O$ decomposition (in the absence of NO) [6,17]. NO thereby functions as a catalyst for $N_2O$ decomposition on iron zeolites. More detailed discussions of the reaction mechanism and the role of the surface oxygen species from $N_2O$ are provided elsewhere [6,8,31].

In Ru-FER, NO is a strong inhibitor for $N_2O$ decomposition; however, the catalyst is very active for the oxidation of NO by $O_2$. Reaction (1) reaches equilibrium already at 560 K. Fe-FER is less active for the oxidation of NO by $O_2$. Thus, the synergistic effect of Fe and Ru can be explained by the reaction sequence

$$2NO + O_2 \rightarrow 2NO_2 \text{ (over Ru)},$$

$$N_2O + NO_2 \rightarrow N_2 + O_2 + NO \text{ (over Fe)},$$

that is, rapid oxidation of NO to $NO_2$ occurs over Ru, and the $NO_2$ enters the $N_2O$ decomposition cycle on Fe. Several arguments do not support this proposal, however. The $NO_2$ concentration on Ru-FER and Fe/Ru-FER is limited by equilibrium (1), which is unfavorable for $NO_2$ at higher temperatures. On Fe-FER, $NO_2$ is formed by reaction (2), which is not equilibrium-limited. As a result, the gas-phase $NO_2$ concentration at higher temperatures is greater on Fe-FER than on Ru-FER and on the bimetallic catalyst; that is, the bimetallic catalyst cannot accelerate the $N_2O$ decomposition cycle over iron by feeding more $NO_2$ to step (2). Moreover, the reaction sequence proposed above depends on the presence of $O_2$ in the feed. However, it has been shown that synergy between Ru and Fe also exists in an $O_2$-free feed mixture [15].

In the absence of $O_2$ in the feed, Ru-FER does not produce any $NO_2$; that is, it is not active for reaction (1). The bimetallic catalyst produces $NO_2$ at low temperature. At higher temperatures, $NO_2$ decomposes to NO and $O_2$ [the reverse reaction of Eq. (1)], and thermodynamic equilibrium among $NO_2$, NO, and $O_2$ is approached. The catalytic behavior of Fe-FER is hardly affected by the presence or absence of $O_2$. This allows us to suggest a different mechanism by which Fe and Ru can cooperate: Fe-FER is very active for the oxidation of NO to $NO_2$ by $N_2O$ [reaction (2)], but $O_2$ formation by reaction of $N_2O$ with $NO_2$ [reaction (2)] is rate-limiting. Ru offers an alternative route for $O_2$ formation by decomposition of $NO_2$ to NO and $O_2$, which is fast (close to equilibrium). The whole reaction sequence can be written as

$$N_2O + NO \rightarrow NO_2 + N_2 \text{ (over Fe)},$$

$$NO_2 \rightarrow NO + (1/2)O_2 \text{ (over Ru)}.$$

This mechanism is in accordance with the kinetic data and could also operate in the presence of $O_2$ in the feed, albeit with lower efficiency.

### 4.2. Adsorptive synergy

The in situ IR data show that a second mechanism may contribute to the synergy between Fe and Ru. The presence of high concentrations of iron influences the sorption properties of NO on the $RuO_2$ particles. In the bimetallic FeRu-FER catalyst, NO adsorbs mainly on the Fe sites (Figs. 7 and 12). Consequently, the coverage of the Ru sites with NO is significantly reduced, especially at high temperatures. NO acts as a strong inhibitor for $N_2O$ decomposition on $RuO_2$. The function of Fe in the bimetallic catalyst is to trap NO and thereby leave the $RuO_2$ surface free to exert its high intrinsic activity for $N_2O$ decomposition. This effect is not observed on the FeRu-FER-2 catalyst with low iron loading. FeRu-FER-2 preferentially adsorbs NO on the Ru component because of the stronger interaction of NO with Ru compared with Fe. Iron can work effectively as an NO trap only if present in high concentrations, that is in large excess and in intimate contact with Ru.

The question may be raised as to whether our IR data are representative, because for experimental reasons they were measured at higher concentrations than the catalytic data. Comparative measurements with similar NO and $N_2O$ concentrations as used for catalysis showed that the spectra do not change much. Between 400 and 800 ppm NO, the adsorption isotherm of NO on iron is rather flat. Under conditions farther away from saturation with NO (i.e., at even lower concentrations or temperatures above 673 K), we can expect NO adsorption to be preferred on Ru rather than on Fe, and the adsorption synergy loses importance.

### 4.3. Redox synergy

$N_2O$ decomposition on iron zeolites proceeds via a redox cycle between $Fe^{2+}$ and $Fe^{3+}$ [32]. Therefore, it is not surprising that the concentration of $Fe^{2+}$ under reaction conditions largely determines the catalytic activity of Fe-ZSM-5 in $N_2O$ decomposition [33]. The concentration of $Fe^{2+}$ becomes even more important in the presence of NO [17], because $Fe^{2+}$ centers act as adsorption sites for NO, which promotes $N_2O$ decomposition over iron zeolites (vide supra). The in situ XANES data show that the fraction of $Fe^{2+}$ sites in a working iron ferrierite catalyst is high, ∼30% if $Fe_2O_3$ particles are excluded. Adding Ru to the catalyst does not increase the concentration of $Fe^{2+}$; in the presence of $O_2$, it even decreases (Table 4). Ru does not have a positive influence on the redox properties of Fe. There is no redox synergy between Fe and Ru.

### 4.4. Comparison of Fe-FER and Fe-ZSM-5

We recently studied NO-assisted $N_2O$ decomposition on a series of Fe-ZSM-5 catalysts [17] and found that the behavior of Fe-FER was markedly different from Fe-ZSM-5. On Fe-ZSM-5, weakly bound surface $NO_2$ species were identified as intermediates in the NO-assisted $N_2O$ decomposition cycle.

Stable surface nitrates did not seem to be involved in the reaction. On Fe-FER, weakly bound surface $NO_2$ species were not identified. Stable, probably charged nitro/nitrate species dominated the IR spectra in the region of 1650–1500 $cm^{-1}$. This indicates that the reaction intermediates on Fe-FER differ from those on Fe-ZSM-5.

A second, marked difference between Fe-FER and Fe-ZSM-5 is in terms of redox activity. The Fe sites in Fe-FER readily reduce to $Fe^{2+}$ (if $Fe_2O_3$ clusters are excluded), whereas XANES measurements on Fe-ZSM-5 show that only a negligible fraction of the iron sites are in the oxidation state $Fe^{2+}$ during reaction with $NO + N_2O$. A more detailed discussion of these effects is beyond the scope of this paper, but we believe that the comparison of Fe-ZSM-5 and Fe-FER merits a more in-depth investigation [34,35].

## 5. Conclusion

The observed synergy between Fe and Ru in bimetallic FeRu-FER catalysts for $N_2O$ decomposition in the presence of NO results from two effects. The first of these effects is a catalytic cooperation between Fe and Ru. The Fe component is very active for the oxidation of NO by $N_2O$, that is, $N_2O + NO \rightarrow NO_2 + N_2$. The subsequent $O_2$ formation via $N_2O + NO_2 \rightarrow O_2 + N_2 + NO$ is rate-limiting. The Ru component offers a second channel for $O_2$ formation, which is rapid: The reaction $NO_2 \leftrightharpoons NO + (1/2)O_2$ is close to equilibrium over Ru. In the forward direction, which is thermodynamically favored at high temperature, it closes the catalytic cycle of $N_2O$ decomposition. In theory, this mechanism should also work for other transition or noble metals that are highly active in the decomposition of $NO_2$ to NO and $O_2$.

A second effect that may contribute to the synergy between Fe and Ru is based on the adsorption properties of the bimetallic catalyst. In a bimetallic sample with high iron loading, NO and $NO_2$-derived surface species adsorb preferentially on the Fe component, thereby significantly reducing the inhibiting effect of NO on the Ru component. The effect is not observed in samples with low iron loadings. Unfortunately, our data do not allow us to quantify the contribution of the adsorption effect to the synergy between Fe and Ru; this would require a more detailed kinetic study. The in situ XANES data show that the presence of Ru does not increase the fraction of $Fe^{2+}$ under reaction conditions; there is no positive influence of Ru on the redox properties of Fe.

## Note added in proof

While this manuscript was being processed, a synergy between Fe and Pt in $N_2O$ decomposition was reported by D. Kaucky, K. Jisa, A. Vondrova, J. Novakova, Z. Sobalik, J. Catal. 242 (2006) 2.

## Acknowledgments

The authors thank Can Pinarci (ETH Zurich) for helping with the IR measurements and Martin Kuba and Dr. Pavel Kukula (ETH Zurich) for participating in the XAS experiments. We also thank Martin Kuba for the Na/K determinations, Dr. Ruud van den Brink (ECN) for valuable discussions, and the reviewers for their constructive comments and suggestions.

## References

[1] M. Kogel, B.M. Abu-Zied, M. Schwefer, T. Turek, Catal. Commun. 2 (2001) 273.
[2] J. Perez-Ramirez, F. Kapteijn, G. Mul, J.A. Moulijn, Chem. Commun. (2001) 693.
[3] J. Perez-Ramirez, F. Kapteijn, G. Mul, J.A. Moulijn, Appl. Catal. B 35 (2002) 227.
[4] A. Guzman-Vargas, G. Delahay, B. Coq, Appl. Catal. B 42 (2003) 369.
[5] J.A.Z. Pieterse, S. Booneveld, R.W. van den Brink, Appl. Catal. B 51 (2004) 215.
[6] J. Perez-Ramirez, F. Kapteijn, G. Mul, J.A. Moulijn, J. Catal. 208 (2002) 211.
[7] C. Sang, C.R.F. Lund, Catal. Lett. 73 (2001) 73.
[8] C. Sang, B.H. Kim, C.R.F. Lund, J. Phys. Chem. B 109 (2005) 2295.
[9] D. Kaucky, Z. Sobalik, M. Schwarze, A. Vondrova, B. Wichterlova, J. Catal. 238 (2006) 293.
[10] B. Neveu, C. Hamon, K. Malefant, French Patent WO 99/34901, 1999.
[11] Y. Li, J.N. Armor, Appl. Catal. B Environ. 1 (1992) L21.
[12] G. Centi, A. Galli, B. Montanari, S. Perathoner, A. Vaccari, Catal. Today 35 (1997) 113.
[13] G. Centi, S. Perathoner, F. Vazzana, M. Marella, M. Tomaselli, M. Mantegazza, Adv. Environ. Res. 4 (2000) 325.
[14] J.A.Z. Pieterse, G. Mul, I. Melian-Cabrera, R.W. van den Brink, Catal. Lett. 99 (2005) 41.
[15] J.A.Z. Pieterse, S. Booneveld, G. Mul, R.W. van den Brink, Stud. Surf. Sci. Catal. 157 (2005) 1915.
[16] V. Boissel, S. Tahir, C.A. Koh, Appl. Catal. B 64 (2006) 234.
[17] G.D. Pirngruber, J.A.Z. Pieterse, J. Catal. 237 (2006) 237.
[18] N. Weiher, E. Bus, B. Gorzolnik, M. Moller, R. Prins, J.A. van Bokhoven, J. Synch. Rad. 12 (2005) 675.
[19] M.S. Kumar, M. Schwidder, W. Grünert, A. Brückner, J. Catal. 227 (2004) 384.
[20] J. Perez-Ramirez, J.C. Groen, A. Brückner, M.S. Kumar, U. Bentrup, M.N. Debbagh, L.A. Villaescusa, J. Catal. 232 (2005) 318.
[21] R.W. van den Brink, S. Booneveld, M.J.F.M. Verhaak, Catal. Today 75 (2002) 227.
[22] A.K. Goel, G. Skorinko, F.H. Pollak, Phys. Rev. B 24 (1981) 7342.
[23] A.P. Alivisatos, Science 271 (1996) 933.
[24] X. Wang, H.Y. Chen, W.M.H. Sachtler, J. Catal. 197 (2001) 281.
[25] K. Hadjiivanov, B. Tsyntsarski, T. Nikolova, Phys. Chem. Chem. Phys. 1 (1999) 4521.
[26] B.R. Wood, J.A. Reimer, A.T. Bell, M.T. Janicke, K.C. Ott, J. Catal. 225 (2004) 300.
[27] K. Hadjiivanov, J. Saussey, J.L. Freysz, J.C. Lavalley, Catal. Lett. 52 (1998) 103.
[28] L.J. Lobree, I.C. Hwang, J.A. Reimer, A.T. Bell, Catal. Lett. 63 (1999) 233.
[29] H.Y. Chen, T. Voskoboinikov, W.M.H. Sachtler, J. Catal. 180 (1998) 171.
[30] Y. Wang, K. Jacobi, G. Ertl, J. Phys. Chem. B 107 (2003) 13918.
[31] G. Mul, J. Perez-Ramirez, F. Kapteijn, J.A. Moulijn, Catal. Lett. 77 (2001) 7.
[32] G.D. Pirngruber, P.K. Roy, Catal. Today 110 (2005) 199.
[33] G.D. Pirngruber, M. Luechinger, P.K. Roy, A. Cecchetto, P. Smirniotis, J. Catal. 224 (2004) 429.
[34] R. Brosius, D. Habermacher, J.A. Martens, L. Vradman, M. Herskowitz, L. Capek, Z. Sobalik, J. Dedecek, B. Wichterlova, V. Tokarova, O. Gonsiorova, Top. Catal. 30–31 (2004) 333.
[35] L. Capek, V. Kreibich, J. Dedecek, T. Grygar, B. Wichterlova, Z. Sobalik, J.A. Martens, R. Brosius, V. Tokarova, Microporous Mesoporous Mater. 80 (2005) 279.